

Supplementary Materials for

**Revealing the Brønsted-Evans-Polanyi relation in halide-activated fast
MoS₂ growth toward millimeter-sized 2D crystals**

Qingqing Ji, Cong Su*, Nannan Mao, Xuezheng Tian, Juan-Carlos Idrobo, Jianwei Miao,
William A. Tisdale, Alex Zettl, Ju Li, Jing Kong*

*Corresponding author. Email: csu@berkeley.edu (C.S.); jingkong@mit.edu (J.K.)

Published 27 October 2021, *Sci. Adv.* **7**, eabj3274 (2021)
DOI: [10.1126/sciadv.abj3274](https://doi.org/10.1126/sciadv.abj3274)

This PDF file includes:

Figs. S1 to S11
Tables S1 to S3

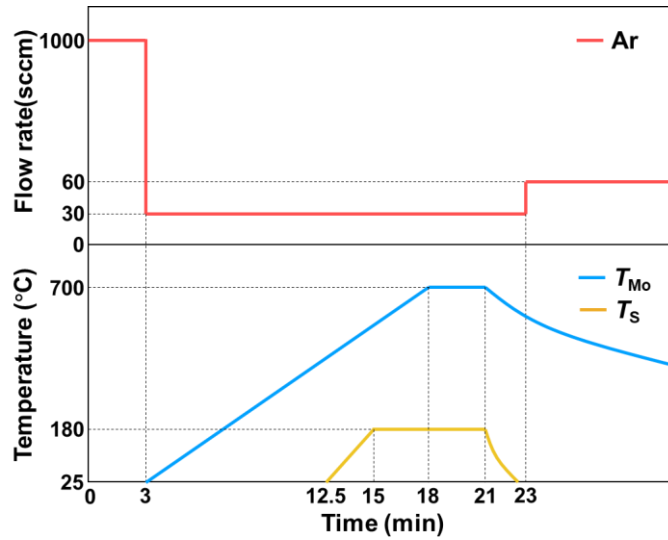


Fig. S1. A typical program of the halide-assisted MoS₂ growth.

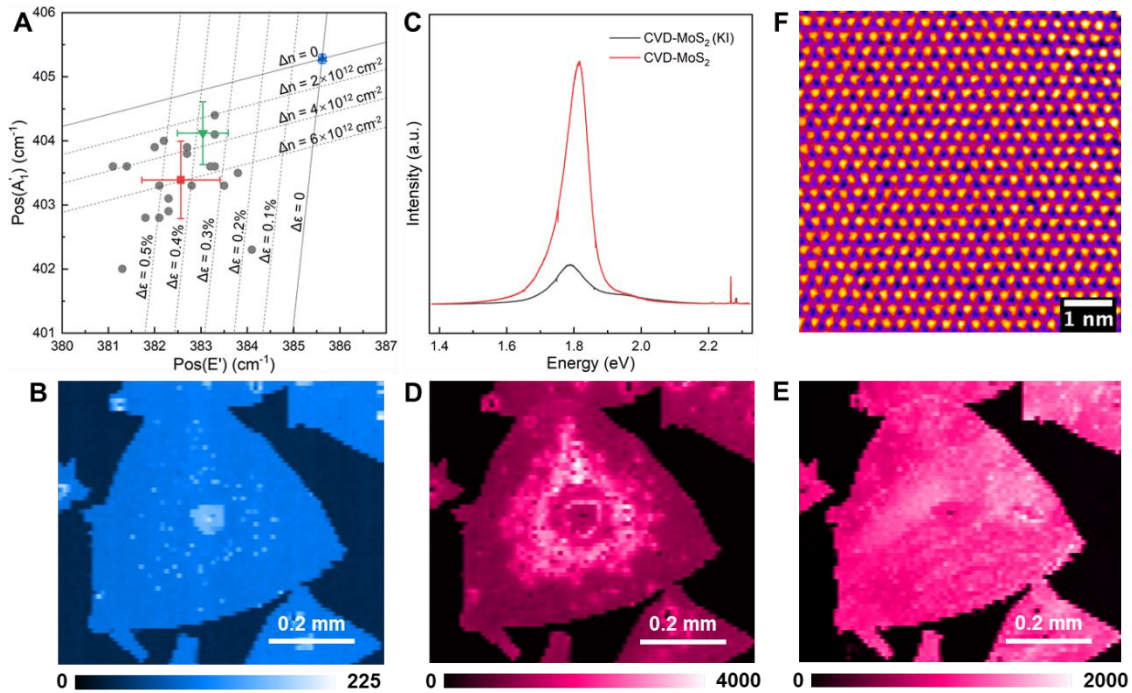


Fig. S2. Characterizations of the KI-assisted grown MoS₂. (A) Raman characterization. The grey circles are data points of the E' and A₁' peak positions. The red square is the average result for our MoS₂ sample, while the green and blue data points are for MoS₂ samples produced by conventional CVD and mechanical exfoliation, respectively. (B) Raman mapping (A₁' peak intensity) image of the large-domain MoS₂ crystal shown in Fig. 1C of the main text. (C) Photoluminescence (PL) spectra of the monolayer MoS₂ samples produced by KI-assisted growth (black) and conventional CVD (red). The weaker PL of the KI-assisted grown sample might be associated with the higher electron doping level as reflected in (A). (D) PL intensity mapping of the 2D MoS₂ crystal in Fig. 1C. (E) PL intensity mapping of the 2D crystal after transfer onto a new SiO₂/Si substrate. The nonuniform PL intensity before transfer might be due to the strain inhomogeneity in the large-size 2D crystal, which is released and contributes to uniform PL after transfer. (F) HAADF image of a representative area of the MoS₂ crystal lattice. No iodine atoms can be seen in the field of view (shown as very bright atoms occupying S sites), proving that they are not involved in the final product at a detectable level. We have imaged quite a number of locations and verified the absence of iodine or potassium

doping.

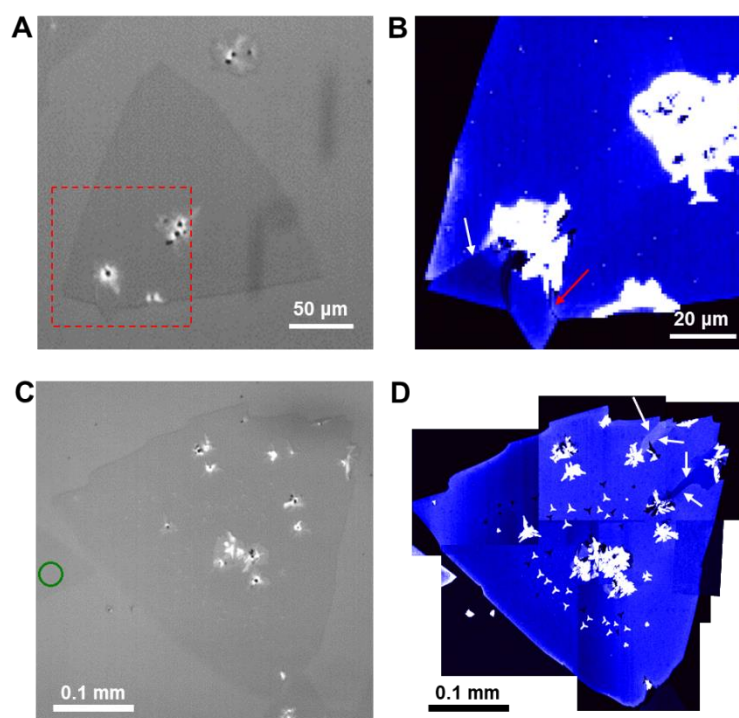


Fig. S3. SHG mapping images of the large-domain MoS₂. (A) Optical image of the 2D MoS₂ crystal same as that in Fig. 1D. (B) Second-harmonic generation mapping of the lower left part in (A), showing grain boundaries (GBs) marked with arrows. Note that the red arrow indicates an antiparallel GB with adjacent areas having identical SHG intensity. (C) Optical image of the 2D crystal with a domain size of ~0.4 mm. (D) Corresponding SHG image of the entire flake by stitching several SHG mapping images. The main body of the 2D flake is free of GBs except at the top right corner (GBs marked with white arrows).

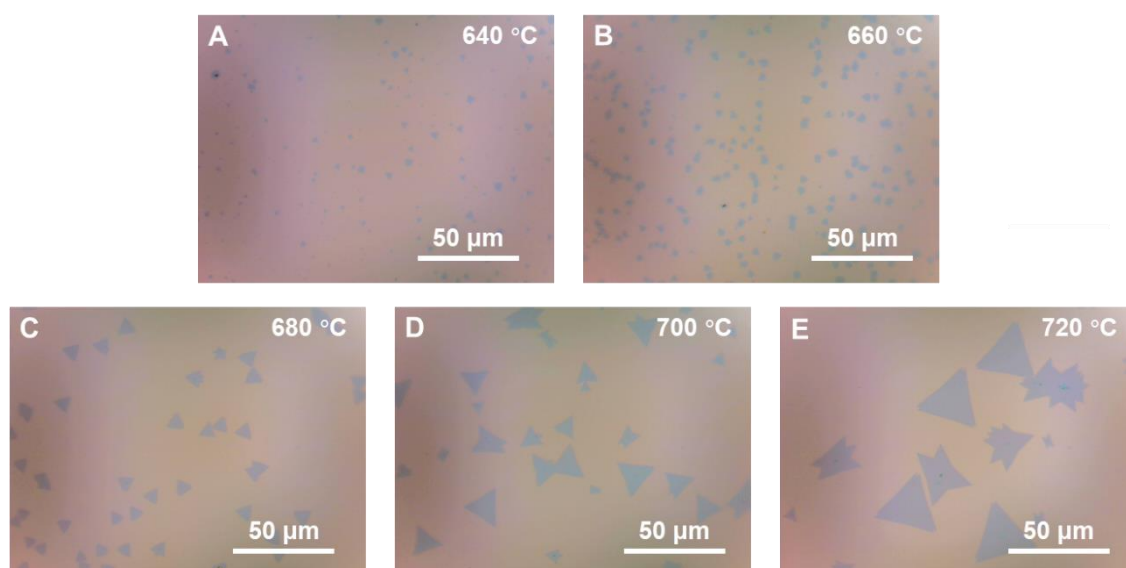


Fig. S4. Optical images of the 2D MoS₂ crystals grown without any halide promoter. Top right of each image

indicates the growth temperature (T_{M0}). Sulfur heating temperature $T_S = 180\text{ }^\circ\text{C}$.

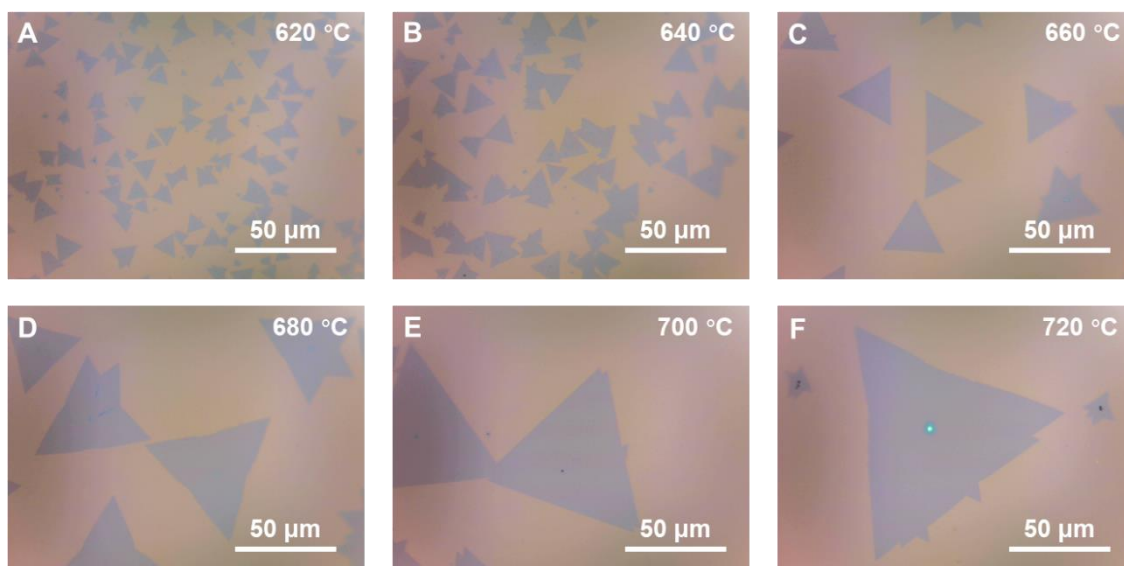


Fig. S5. Optical images of the 2D MoS₂ crystals grown with KI promoter. Top right of each image indicates the growth temperature. Sulfur heating temperature $T_S = 180\text{ }^\circ\text{C}$.

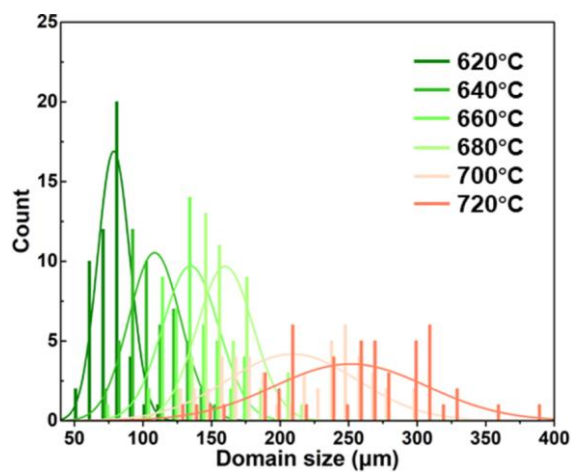


Fig. S6. Domain size statistics of the 2D MoS₂ crystals grown with KI promoter at $T_S = 170\text{ }^\circ\text{C}$.

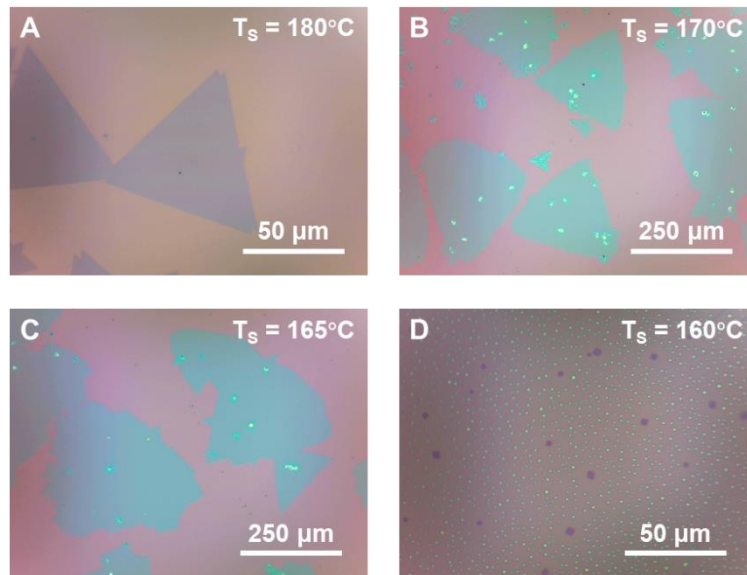


Fig. S7. Optical images of the 2D MoS₂ crystals grown with KI promoter at $T_{Mo} = 700$ °C. Top right of each image indicates the sulfur heating temperature. The green particles in the lower right image are likely the unsulfurized potassium molybdate droplets. This result is similar to the surface morphology grown without sulfur supply.

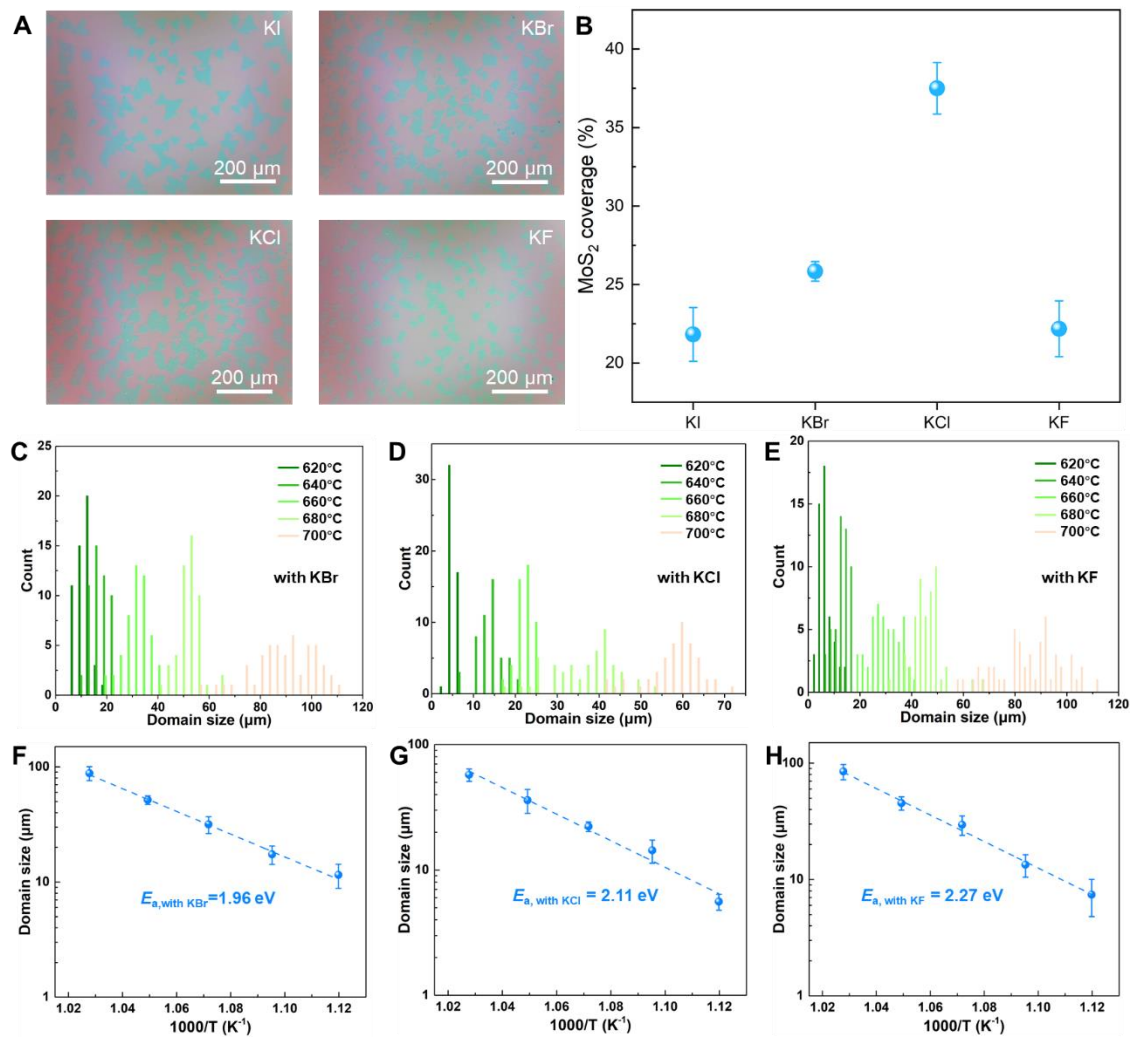


Fig. S8. MoS₂ growth results assisted by different halide salts. (A) Optical images of MoS₂ grown at 680 °C with

presence of different potassium halides. **(B)** Calculated MoS₂ coverage dependent on the salts. **(C-E)** T_{Mo} -dependent domain size statistics of the 2D MoS₂ crystals grown with **(C)** KBr, **(D)** KCl, and **(E)** KF promoters. **(F-H)** Corresponding Arrhenius plots of the average domain size versus $1000/T$ for the three cases. The derived reaction barriers are found to increase in the sequence of KI (1.80 eV, Fig. 2B in the main text), KBr (1.96 eV), KCl (2.11 eV), and KF (2.27 eV).

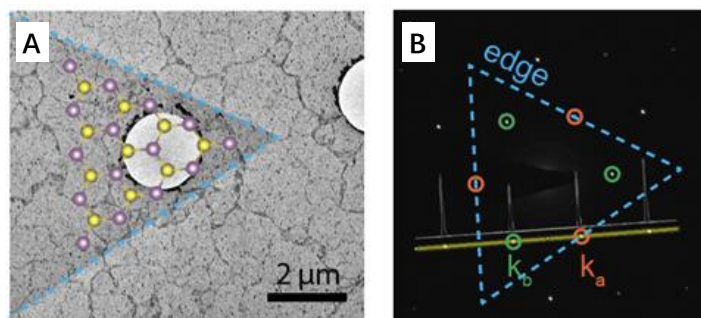


Fig. S9. Determining the MoS₂ edge type by electron diffraction. Large field-of-view TEM image on the edge of a 2D MoS₂ crystal **(A)** and corresponding SAED pattern **(B)**. The extracted line profile categorizes the first-order diffraction points into two groups by intensity, which are marked with green and orange circles. The higher-intensity group (k_a), which point towards the flake edges, are associated with zigzag-Mo edge type.

Table S1. The Mo edges passivated by halogen atoms and oxygen.

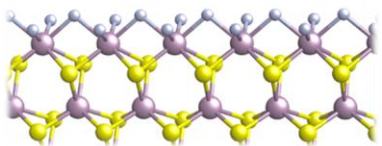
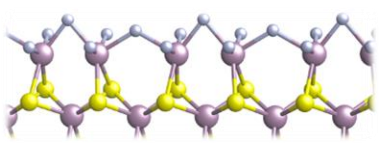
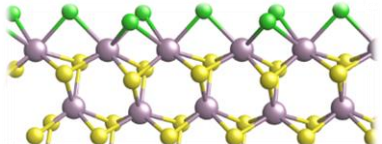
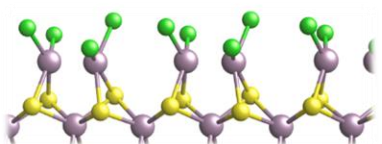
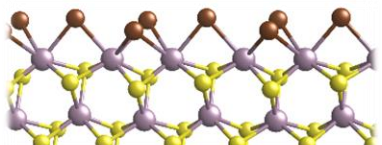
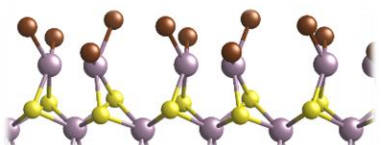
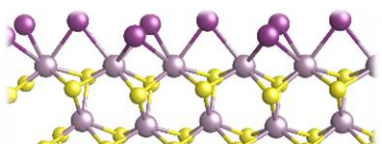
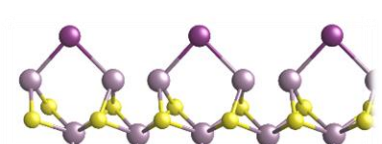
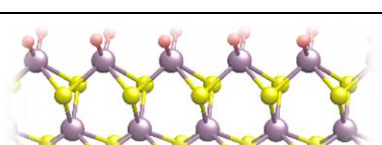
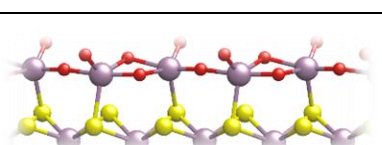
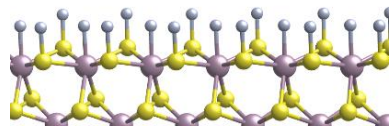
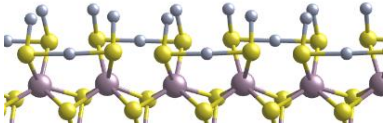
	zigzag Mo edge	antenna Mo edge
F		
Cl		
Br		
I		
O		

Table S2. The S edges stabilized by halogen atoms and oxygen.

	zigzag S edge	antenna S edge
F		
Cl, Br, I, O	Not stable	Not stable

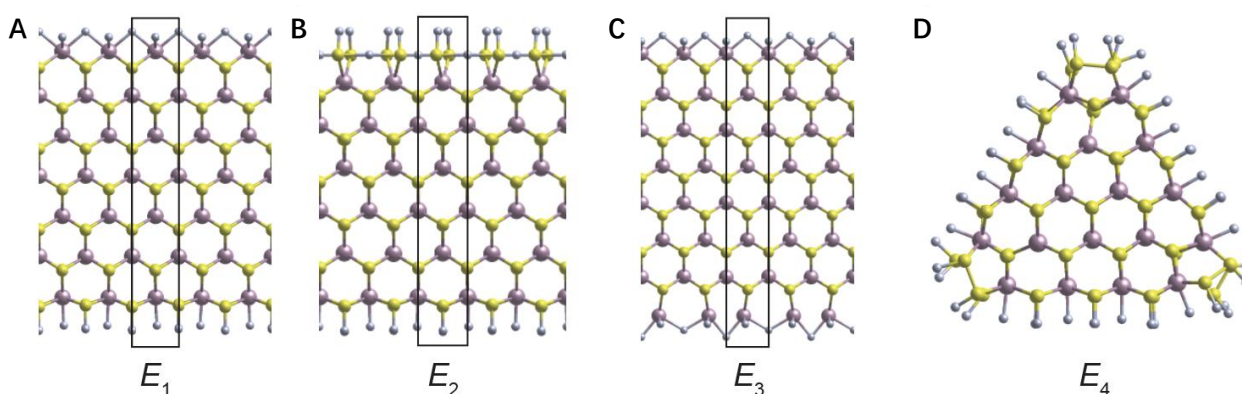


Fig. S10. The nanostructures used for calculating the formation energies of different edges. The above images are examples of F-passivated edges which include (A) zigzag-Mo and zigzag-S; (B) antenna-S and zigzag-S; (C) zigzag-Mo and antenna-Mo; and (D) the nano-island including zigzag-S and antenna-S. The unit length used for defining the edge formation energy has been marked by black rectangles in these images.

Table S3. List of N_1 , N_2 , N_3 , and N_4 numbers for calculating the edge formation energies by Eq. (3).

	N_1	N_2	N_3	N_4
F	6	6	6	45
Cl	1.5	0	3.5	0
Br	1.5	0	3.5	0
I	1.5	0	2	0
O	2	0	4.5	0

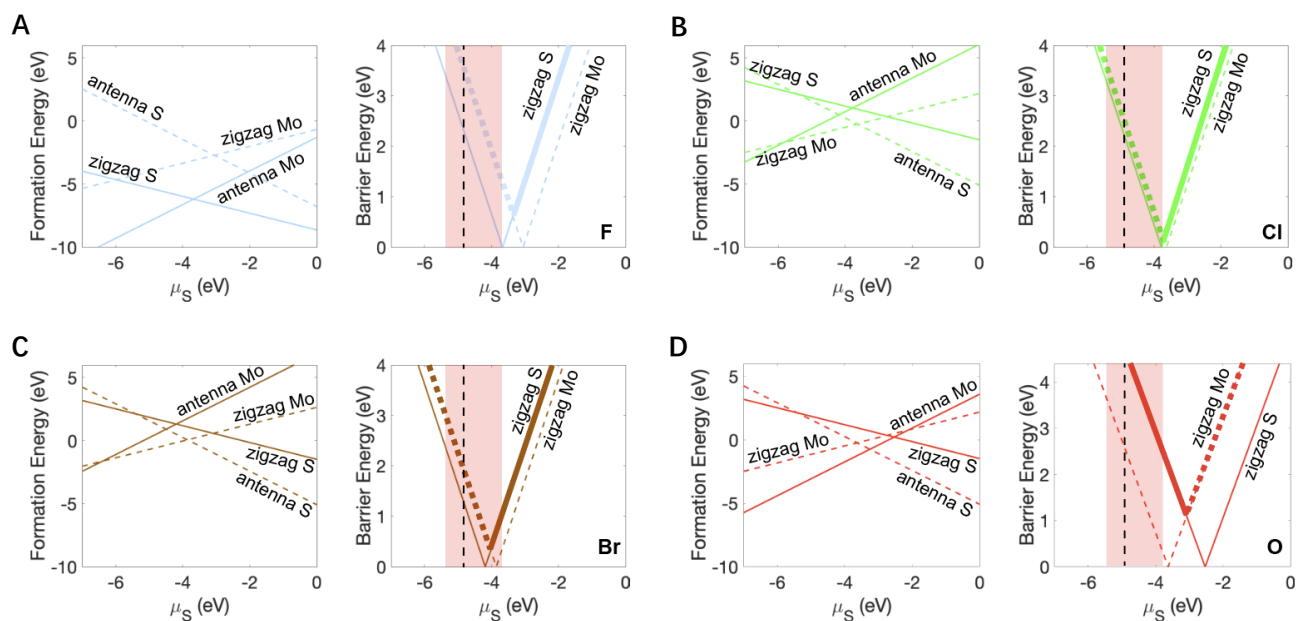


Fig. S11 DFT calculations of the MoS₂ growth reaction barriers. The calculations are based upon (A) fluorine, (B) chlorine, (C) bromine, and (D) oxygen edge passivation. Each left panel exhibits the formation energies of the four kinds of edges (zigzag-Mo, antenna-S, zigzag-S, and antenna-Mo), whose atomic configurations passivated by halogen/oxygen is depicted in Table S1 and S2. Shaded regions in the right panels indicate accessible μ_S , and the vertical dash lines mark the position of $\mu_S = -4.9$ eV that we use to find the halogen-dependent reaction barriers for the plot of Fig. 4C in the main text.